

# Axion Stars Nucleation in Dark Mini-Halos around Primordial Black Holes

Mark P. Hertzberg<sup>1\*</sup>, Enrico D. Schiappacasse<sup>2,3†</sup>, Tsutomu T. Yanagida<sup>3‡</sup>

<sup>1</sup>*Institute of Cosmology, Department of Physics and Astronomy, Tufts University, Medford, MA 02155, USA*

<sup>2</sup>*Department of Physics, P.O.Box 35 (YFL), FIN-40014 University of Jyväskylä, Finland*

<sup>3</sup>*Tsung-Dao Lee Institute & School of Physics and Astronomy, Shanghai Jiao Tong University, 200240 Shanghai, China*

We consider a general class of axion models, including the QCD and string axion, in which the PQ symmetry is broken before or during inflation. Assuming the axion is the dominant component of the dark matter, we discuss axion star formation in virialized dark mini-halos around primordial black holes through gravitational Bose-Einstein condensation. We determine the conditions for mini-halos to kinetically produce axion stars before galaxy formation. Today, we expect up to  $\sim 10^{17}$  ( $\sim 10^9$ ) axion stars in a radius of 100 parsecs around the sun for the case of the QCD (string) axion.

## INTRODUCTION

By considering shortcomings in the Standard Model of particle physics, the axion is one of the strongest dark matter candidates [1–4]. In the scenario at which the PQ symmetry is broken after inflation, the axion field initially take random values from one Hubble patch to the next leading to large isocurvature perturbations in the axion energy density at the QCD phase transition. These overdensities will decouple from the Hubble flow and form the so-called axion miniclusters [5–7].

However, the scenario at which the PQ symmetry is broken after inflation is in strong tension with numerical simulations reported in [8]. The additional axion abundance coming from the decay of topological defects significantly changes the usual axion abundance coming from the misalignment mechanism [9, 10]. Only when the domain wall number ( $N_{\text{DW}}$ ) is equal to the unity, the axion can be the cold dark matter in the Universe in the narrow mass range  $m_a = (0.8 - 1.3) \times 10^{-4}$  eV. If  $N_{\text{DW}} > 1$ , the QCD axion is excluded.

In this letter, we consider a more general class of the axion model, including the string axion, where the PQ symmetry is broken during or before the inflation. In this case, we have the so-called isocurvature perturbation problem [11–16], but there are many solutions to this (see, for example, [17]). If this is the case, density fluctuations of the axion dark matter are sufficiently small.

In particular, we discuss the formation of axion stars<sup>1</sup> in dark-mini halos around primordial black holes (PBHs) through gravitational Bose-Einstein condensation (BEC) in the kinetic regime. PBHs [26–30] behave as cold dark

matter and are stable for sufficiently large masses. Nowadays, their possible existence has been strongly revitalized since the first detection of two merging black holes by the LIGO-Virgo collaboration [31]. Since PBHs are local overdensities in the dark matter distribution, they naturally act as seeds for dark matter structures formation. In the scenario at which the axion is the dominant component of the dark matter, dark mini-halos will unavoidably grow around PBHs. If PBHs exist, this scenario is realized whatever the fundamental nature of original axion dark matter distribution is.

The kinetic formation of axion stars in these dark mini-halos, where the axion field coherence length is much smaller than the halo radius, depends on the halo energy density as well as the axion mass and velocity. Neglecting a weak logarithm dependence, the time scale for axion star nucleation runs as  $\tau_{\text{gr}} \sim m_a^3 v_a^6 \rho_{\text{halo}}^{-2}$ , where  $m_a$  and  $v_a$  refer to the axion mass and velocity, respectively, and  $\rho_{\text{halo}}$  is the halo energy density [32]. In this letter, we show accretion of axion dark matter around PBHs is effective enough to achieve axion stars formation before dressed PBHs begin to interact with non-linear structures.

## DARK MINI-HALOS AROUND PBHS

Primordial black holes which are formed with a mass  $M_{\text{PBH}} \gtrsim 10^{15}$  gram do not evaporate but begin to form compact dark matter halos by accreting the surrounding axion dark matter.

Any overdensity within a sphere in an expanding Universe will seed the growth of a mini-halo according to the theory of spherical gravitational collapse [33]. Under the assumption that each PBH is stationary and isolated, and dark matter background is initially in the Hubble flow, analytical and numerical calculations [34] show PBH dark halo mainly growth during the matter-dominated era reaching up to  $\sim 10^2 M_{\text{PBH}}$  in units of the

<sup>1</sup> Axion star is a particular kind of boson star (see [18] for a review about boson stars and [19–21] for novel extensions) corresponding to self-gravitating bound states of an axion Bose-Einstein condensation [22–25].

central PBH mass. The dark halo mass and radius grow as [34, 35]

$$M_{\text{halo}}(z) = 3 \left( \frac{1000}{1+z} \right) M_{\text{PBH}}, \quad (1)$$

$$R_{\text{halo}}(z) = 0.019 \text{ pc} \left( \frac{M_{\text{halo}}}{M_{\odot}} \right)^{1/3} \left( \frac{1000}{1+z} \right). \quad (2)$$

Both expressions agree very well with calculations of the virial mass and radius performed in [36]. These relations hold until the time of first galaxies formation at  $z \sim 30$ , when dressed PBHs begin to interact with non-linear structures.

We need to compare the axion de Broglie wavelength  $\lambda_{\text{DB}}$  with the halo radius to see the validity of the above equations. In particular, we have

$$\frac{\lambda_{\text{DB}}}{R_{\text{halo}}} \sim 10^{-12} \left( \frac{10^{-5} \text{ eV}}{m_a} \right) \left( \frac{M_{\odot}}{M_{\text{PBH}}} \right)^{2/3} \left( \frac{1+z}{1000} \right)^{7/6}, \quad (3)$$

where we have taken  $v_a \sim (G_N M_{\text{halo}}/R_{\text{halo}})^{1/2}$  as an estimate of the axion virial velocity. When  $\lambda_{\text{DB}}/R_{\text{halo}} \gtrsim 1$  quantum effects of the dark matter particle cannot be ignored. We expect that at that regime, the accretion of dark matter from PBHs is not efficient.

## AXION STARS NUCLEATION

Lattice simulations performed by Levkov et al. [32] show axion stars may nucleate kinetically in virialized dark matter halos/axion miniclusters through gravitational BEC.<sup>2</sup> At large occupation numbers, the system is described by a random classical field which evolves under its own gravitational potential. The kinetic regime require to satisfy the following conditions:

$$(m_a v_a) \times (R_{\text{halo}}) \gg 1, \quad (4)$$

$$(m_a v_a^2) \times (\tau_{\text{gr}}) \gg 1. \quad (5)$$

Here  $\tau_{\text{gr}}$  is the condensation time scale for the axion star formation. This time scale is proportional to the inverse of the kinetic relaxation rate  $\Gamma_{\text{kin}} \sim n_a \sigma_{\text{gr}} v_a \mathcal{N}$ , where  $n_a$  is the halo axion number density,  $\sigma_{\text{gr}} \approx 8\pi m_a^2 G_N^2 \Lambda / v_a^4$  is the scattering cross section due to gravitational interaction, and  $\mathcal{N} = (6\pi^2 n_a) / (m_a v_a)^3$  is the occupancy number related to Bose enhancement. Here  $\Lambda \equiv \log_e(m_a v_a R_{\text{halo}})$  is the Coloumb logarithm.

This relaxation rate differs from the other gravitational rate which appears in classical field theory within the so-called condensation regime,  $\Gamma_{\text{cond}} \sim 8\pi G_N m_a^2 n_a / k^2$

where  $k$  is some characteristic wave number [22, 37]. Usually the condensation relaxation rate is larger than the kinetic relaxation rate since  $\Gamma_{\text{cond}}$  scales like  $G_N$  but  $\Gamma_{\text{kin}}$  scales like  $G_N^2$ .

In the kinetic regime,  $\tau_{\text{gr}}$  is calculated to be [32]

$$\tau_{\text{gr}} = \frac{b\sqrt{2}m_a^3 v_a^6}{12\pi^3 G_N^2 \rho_{\text{halo}}^2 \Lambda}, \quad (6)$$

$$\bar{\tau}_{\text{gr}} \simeq \frac{4\sqrt{2}}{27\pi} \left( \frac{R_{\text{halo}}}{v_a} \right) (R_{\text{halo}} m_a v_a)^3, \quad (7)$$

where  $\bar{\tau}_{\text{gr}} \equiv \tau_{\text{gr}} \Lambda$ . The numerical coefficient  $b = \mathcal{O}(1)$  depends on the details of the process. To obtain Eq. (7), we have taken  $b = 1$  and  $v_a^2 \sim (4\pi/3) G_N \rho_{\text{halo}} R_{\text{halo}}^2$ .

Even though we will use Eq. (7) as our standard time scale for axion stars nucleation, this time needs to be considered with caution. Numerical results reported in [38] show stars nucleation in axion miniclusters occurs at least  $\sim \mathcal{O}(10^2)$  times earlier than the time scale predicted by  $\tau_{\text{gr}}$ . This situation suggests that the true relaxation rate places somewhere between  $\Gamma_{\text{cond}}$  and  $\Gamma_{\text{kin}}$ .

We apply Eqs. (4, 5, 7) to analyze axion stars nucleation in dark mini-halos of dressed PBHs. For numerical calculations, we consider a flat  $\Lambda$ CDM cosmology and used values based on Planck TT,TE,EE+lowE+lensing+BAO at the 68% confidence levels in [39]. Using Eqs. (1, 2) and  $v_a \sim (G_N M_{\text{halo}}/R_{\text{halo}})^{1/2}$ , we reexpress Eqs. (4, 5, 7) as

$$\frac{m_a v_a R_{\text{halo}}}{10^\alpha} \simeq \left( \frac{m_a}{10^{-5} \text{ eV}} \right) \left( \frac{1000}{1+z} \right)^{7/6} \left( \frac{M_{\text{PBH}}}{10^{-10} M_{\odot}} \right)^{2/3}, \quad (8)$$

$$\frac{m_a v_a^2 \bar{\tau}_{\text{gr}}}{10^\beta} \simeq \left( \frac{m_a}{10^{-5} \text{ eV}} \right)^4 \left( \frac{1000}{1+z} \right)^{14/3} \left( \frac{M_{\text{PBH}}}{10^{-10} M_{\odot}} \right)^{8/3}, \quad (9)$$

$$\frac{\bar{\tau}_{\text{gr}}}{10^\gamma} \simeq \text{Gy} \left( \frac{m_a}{10^{-5} \text{ eV}} \right)^3 \left( \frac{1000}{1+z} \right)^5 \left( \frac{M_{\text{PBH}}}{10^{-10} M_{\odot}} \right)^2. \quad (10)$$

where  $\alpha \equiv \log(2.1 \times 10^4)$ ,  $\beta \equiv \log(1.3 \times 10^{16})$ , and  $\gamma \equiv \log(2.5 \times 10^7)$ . Take  $m_a \equiv 10^{-(5+x)} \text{ eV}$ ,  $z \equiv (10^3)/(10^z) - 1$ ,  $M_{\text{PBH}} \equiv 10^{-(10+y)} M_{\odot}$  to replace them into Eqs. (8, 9, 10). Define  $(m_a v_a R_{\text{halo}}) = 10^C$ ,  $(m_a v_a^2 \bar{\tau}_{\text{gr}}) = 10^B$ , and  $(\bar{\tau}_{\text{gr}}) = 10^A \text{ Gyr}$ . We obtain

$$m_a v_a R_{\text{halo}} \simeq 10^{C_{\text{min}}}, \quad (11)$$

$$m_a v_a^2 \bar{\tau}_{\text{gr}} \simeq \frac{0.43}{C_{\text{min}}} 10^{B_{\text{min}}}, \quad (12)$$

$$\bar{\tau}_{\text{gr}} \simeq \frac{0.43}{C_{\text{min}}} 10^{A_{\text{min}}}, \quad (13)$$

where  $A_{\text{min}} = (\gamma - 3\beta/4) + 3B_{\text{min}}/4 + 3\bar{z}/2$  and  $C_{\text{min}} = (\alpha - \beta/4) + B_{\text{min}}/4$ . At a given redshift, once  $B_{\text{min}}$  is set,

<sup>2</sup> In the whole set up of [32], axions are considered as nonrelativistic bosons which interact themselves via gravitation neglecting the axion self-interaction.

Eqs. (11,12,13) are automatically set together to a linear relation between  $M_{\text{PBH}}$  and  $m_a$ . In details, we have

$$\log \left[ \left( \frac{m_a}{10^{-5} \text{ eV}} \right)^{3/2} \right] = -\frac{3}{8}\beta + \frac{3}{8}B_{\text{min}} - \frac{7}{4}\log \left[ \frac{10^3}{1+z} \right]. \quad (14)$$

As we go deep in the kinetic regime, the condensation time increases as well as the related axion mass ( $M_{\text{PBH}}$ ) for fixed  $M_{\text{PBH}}$  ( $m_a$ ).

Using Eqs. (11,12), we show in Fig. 1 contour-levels of  $(m_a v_a R_{\text{halo}}, m_a v_a^2 \tau_{\text{gr}})$  at a given redshift  $z$  in the parameter space  $(M_{\text{PBH}}, m_a)$ . Blue solid ( $z = z_{\text{eq}}$ ) and dashed ( $z = 894$ ) lines correspond to  $(m_a v_a R_{\text{halo}}, m_a v_a^2 \tau_{\text{gr}}) \sim (10^2, 10^6)$  and  $\sim (50, 10^5)$ , respectively. The blue shaded region between these two lines shows the parameter space of  $(M_{\text{PBH}}, m_a)$  at  $894 < z < z_{\text{eq}}$  satisfying the kinetic regime as  $(m_a v_a R_{\text{halo}}, m_a v_a^2 \tau_{\text{gr}}) \gtrsim (50, 10^5)$ . Using Eq. (13), we estimate the corresponding condensation time scales which range as  $\sim (10^{-2} - 10^{-1})$  Gyr, so that  $\tau_{\text{gr}}(z) \lesssim t(z \simeq 30) - t(z)$ .

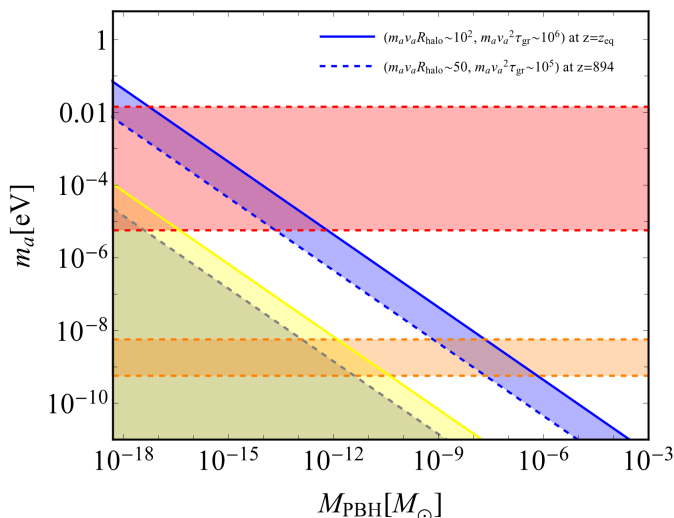


FIG. 1. Contour-levels of  $(m_a v_a R_{\text{halo}}, m_a v_a^2 \tau_{\text{gr}})$  at a given redshift  $z$  in the parameter space  $(M_{\text{PBH}}, m_a)$ . The blue shaded region between the blue solid ( $z = z_{\text{eq}}$ ) and dashed ( $z = 894$ ) lines corresponds to the parameter space of  $(M_{\text{PBH}}, m_a)$  at  $894 < z < z_{\text{eq}}$  which satisfies the kinetic regime as  $(m_a v_a R_{\text{halo}}, m_a v_a^2 \tau_{\text{gr}}) \gtrsim (50, 10^5)$ . The intersection between the red (orange) band and the blue shaded region corresponds to the parameter space for the QCD (string) axion, where  $4 \times 10^8 \text{ GeV} \gtrsim F_a \gtrsim 10^{12} \text{ GeV}$  [40, 41] (where  $10^{15} \text{ GeV} \gtrsim F_a \gtrsim 10^{16} \text{ GeV}$  [42, 43]). The yellow solid (gray dashed) line plus the yellow (gray) shaded region correspond to the zone in which  $\lambda_{\text{DB}}/R_{\text{halo}} \geq 1$  at  $z_{\text{eq}}$  (at  $z = 894$ ) [see Eq. (3)].

The intersection between the red (orange) band and the blue shaded region show the parameter space  $(M_{\text{PBH}}, m_a)$  associated with axion stars nucleation for

the case of the QCD (string) axion. For the QCD axion, PBHs with masses  $5 \times 10^{-19} M_{\odot} \lesssim M_{\text{PBH}} \lesssim 7 \times 10^{-13} M_{\odot}$  are able to form an axion dark mini-halo which satisfies the kinetic regime at a given redshift  $z_{\text{eq}} \leq z \leq 894$ . For the case of the string axion, the central PBHs are heavier with a mass range of  $7 \times 10^{-10} M_{\odot} \lesssim M_{\text{PBH}} \lesssim 7 \times 10^{-7} M_{\odot}$ .

The yellow solid (gray dashed) line plus the yellow (gray) shaded region show the parameter space at  $z = z_{\text{eq}}$  ( $z = 894$ ) in which the accretion of axion dark matter from PBHs is not efficient, e.g.  $\lambda_{\text{DB}}/R_{\text{halo}} \geq 1$  [see Eq. (3)]. We see the particle-like behavior of the QCD and string axions in the parameter space of interest is strong enough to ensure their accretion from PBHs. Indeed, the axion particle-like behavior is a requirement to satisfy the kinetic regime as shown in Eq. (4).

Since at small radii dark mini-halos have a large spherically symmetric density showing a steep  $r^{-9/4}$  density profile [36, 44], we expect stars nucleation mainly occur in the inner region of these halos.

In the case that nucleated axions stars correspond to excited states coming from radial perturbations, we expect they tend to settle down at the ground state configuration by ejecting part of the axion particles to eliminate the excess of kinetic energy [45].<sup>3</sup>

Suppose that at redshift  $z$ , the dark mini-halo satisfies conditions for axion stars nucleation with a condensation time  $\tau_{\text{gr}}(z)$ . Thus, the present average parameter density of axion stars is given by

$$\Omega_{\star,0} = \left( \frac{N_{\star} M_{\star}}{M_{\text{PBH}}} \right) \xi_{\text{DM}}^{\text{PBH}} \Omega_{\text{DM},0} \quad (15)$$

where  $N_{\star}$  is the average number of axion stars per halo after nucleation,  $\Omega_{\text{DM},0}$  is the present dark matter parameter density,  $\xi_{\text{DM}}^{\text{PBH}} \equiv \Omega_{\text{PBH}}/\Omega_{\text{DM}}$  is the fraction of dark matter in PBHs, and  $M_{\star}$  is the characteristic mass of axion stars.

Axion stars after nucleation continue capturing axions from the halo until the growth rate slow downs and saturates [32, 38]. We estimate this mass after saturation by equating the virial velocity of the halo at the nucleation time, e.g.  $v_a \sim (G_N M_{\text{halo}}/R_{\text{halo}})^{1/2}$ , to the virial velocity in the gravitational potential of the axion star, e.g.  $v_{\star} \simeq (G_N M_{\star} m_a/\hbar)$  [46], according to

$$\left( \frac{M_{\star}}{M_0} \right) \simeq (1+z_{\star})^{1/2} \left( \frac{M_{\text{halo}}}{M_0} \right)^{1/3}, \quad (16)$$

where  $M_0 \simeq 5.5 \times 10^{-19} M_{\odot} (10^{-5} \text{ eV}/m_a)^{3/2}$ . Up to a numerical factor of order one, the same scaling relation was previously found for solitonic cores in halos

<sup>3</sup> By using different initial conditions, numerical simulations performed in [38] found axion stars nucleation in highly excited states with non-radial oscillations.

of fuzzy dark matter [47]. By using Eq. (1), we can rewrite Eq. (16) in terms of the mass of the central PBH to obtain  $(M_\star/\bar{M}_0) \simeq (1+z_\star)^{1/6}(M_{\text{PBH}}/\bar{M}_0)^{1/3}$ , where  $\bar{M}_0 = \sqrt{3000}M_0$ . Since this mass shows a very weak dependence on the redshift, we take  $M_\star \sim (M_{\text{PBH}}^{1/2}\bar{M}_0)^{2/3}$  as the characteristic mass of axion stars in Eq. (15).

Axion stars nucleation could occur simultaneously in different places of the dark mini-halo so that  $N_\star$  in Eq. (15) may be much greater than one. At the nucleation time, the maximum number of nucleated stars can be roughly estimated as  $N_\star^{\text{max}} \sim M_{\text{halo}}/M_\star$ . Thus, using Eq. (15), the present average parameter density of axion stars may take values within the range

$$\left(\frac{\bar{M}_0}{M_{\text{PBH}}}\right)^{2/3} \xi_{\text{DM}}^{\text{PBH}} \Omega_{\text{DM},0} \lesssim \Omega_{\star,0} \lesssim \left(\frac{3000}{1+z_\star}\right) \xi_{\text{DM}}^{\text{PBH}} \Omega_{\text{DM},0}. \quad (17)$$

Figure 2 shows contour-levels of  $(m_a v_a R_{\text{halo}}, m_a v_a^2 \tau_{\text{gr}})$  in the parameter space  $(m_a, M_\star)$  for the QCD (red band) and the string (orange band) axion case. The blue solid ( $z = z_{\text{eq}}$ ) and dashed ( $z = 894$ ) lines refer to the values  $(m_a v_a R_{\text{halo}}, m_a v_a^2 \tau_{\text{gr}}) \sim (10^2, 10^6)$  and  $\sim (50, 10^5)$ , respectively. The blue shaded region between these two lines refers to the parameter space of  $(m_a, M_\star)$  at which the kinetic regime is satisfied as  $(m_a v_a R_{\text{halo}}, m_a v_a^2 \tau_{\text{gr}}) \gtrsim (50, 10^5)$  at  $z_{\text{eq}} < z < 894$ . For the case of the QCD axion, axion stars masses after saturation range as  $\mathcal{O}(10^{-20}) M_\odot \lesssim M_\star \lesssim \mathcal{O}(10^{-15}) M_\odot$ . When dark mini-halos are composed by the string axion, axion stars masses are heavier ranging as  $\mathcal{O}(10^{-11}) M_\odot \lesssim M_\star \lesssim \mathcal{O}(10^{-9}) M_\odot$ . In principle,  $M_\star$  can still grow after the saturation point although at a very suppressed rate [38]. The maximum mass reachable for a stable axion star in the ground state configuration reads as  $M_{\text{max},\star} \sim 7 \times 10^{-12} M_\odot (10^{-5} \text{ eV}/m_a)^2$  [23], which is shown with a red solid line in Fig. 2. We see axion stars inside mini-halos will not reach (and overpass)  $M_\star^{\text{max}}$  avoiding collapse and explosion in relativistic axions [48].

The mass of PBHs can be associated with observational constraints leading to an upper bound on the fraction of dark matter that PBHs can explain,  $\xi_{\text{DM,max}}^{\text{PBH}}$  [49–54]. We consider in Eq. (17) a conservative maximum fraction of dark matter in PBHs as  $\xi_{\text{DM}}^{\text{PBH}} = \min(\xi_{\text{DM,max}}^{\text{PBH}}, Q)$ , where  $Q$  is predefined. Nucleated axion stars may potentially be constrained through femtolensing and microlensing events for the case of the QCD and string axion, respectively. However, their physical radius are larger than the Einstein ring radius and an extended mass function of non-point like compact object needs to be considered to place observational constraints.<sup>4</sup> We leave the study of this possibility for future work.

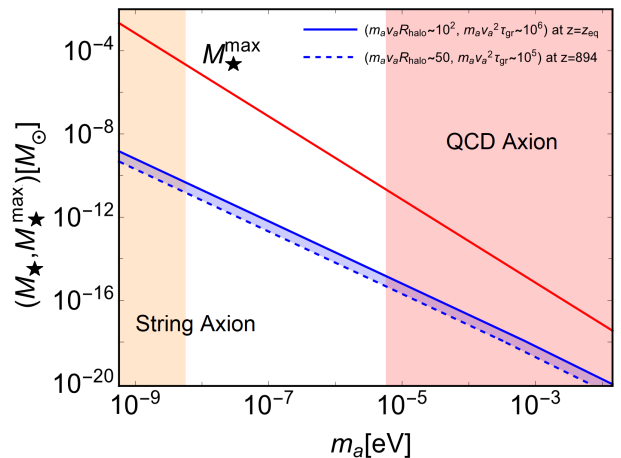


FIG. 2. Contour-levels of  $(m_a v_a R_{\text{halo}}, m_a v_a^2 \tau_{\text{gr}})$  in the parameter space  $(m_a, M_\star)$ . The blue shaded region between the blue solid ( $z = z_{\text{eq}}$ ) and dashed ( $z = 894$ ) lines corresponds to the parameter space of  $(m_a, M_\star)$  at which the kinetic regime is satisfied as  $(m_a v_a R_{\text{halo}}, m_a v_a^2 \tau_{\text{gr}}) \gtrsim (50, 10^5)$  at  $z_{\text{eq}} < z < 894$ . Red (orange) band corresponds to the mass range for the QCD (string) axion. The red solid line indicates the theoretical maximum mass,  $M_\star^{\text{max}}$ , that an axion star in the ground state configuration can achieve [23].

The blue (gray) shaded region in Fig. 3 shows an estimate of the current fraction of dark matter in axion stars,  $\xi_{\text{DM}}^*$ . We have used Eq. (17), a fraction of dark matter in PBHs no greater than 0.5% (10%), the contour level of  $(m_a v_a R_{\text{halo}}, m_a v_a^2 \tau_{\text{gr}}) \sim (10^2, 10^6)$  at  $z = z_{\text{eq}}$ , and a nucleation time of  $z_\star \sim 800$  much more earlier than that predicted by the condensation time scale in Eq. (13). Red and orange bands correspond to axion star masses associated with the QCD axion and the string axion case, respectively. Numerical simulations are required to determine with accuracy the relation  $M_\star = M_\star(M_{\text{halo}})$  and the parameter space  $(M_{\text{PBH}}, m_a)$  associated with axion stars nucleation.

## DISCUSSION

Suppose conditions in dark mini-halos for formation of axion stars are satisfied such that they are formed before the time of first galaxies formation,  $z_\star \sim 30$ . We expect galactic halos at the time of formation around  $z \sim 6$  would be composed by isolated and clustered dressed PBHs (containing axion stars), naked PBHs, and axion stars as well as smooth axion dark matter background.

We discuss in [57] the possibility of a significant part of the dark matter background ends up localized in the form of dark mini-halos around PBHs within galactic halos and effects of this on dark matter direct detection (see [58] for the general status of direct and indirect dark matter searches). The nucleation of axion stars in these dark mini-halos addresses in this article would comple-

<sup>4</sup> Femtolensing and microlensing observational constraints for the case of axion miniclusters are discussed in [55, 56].

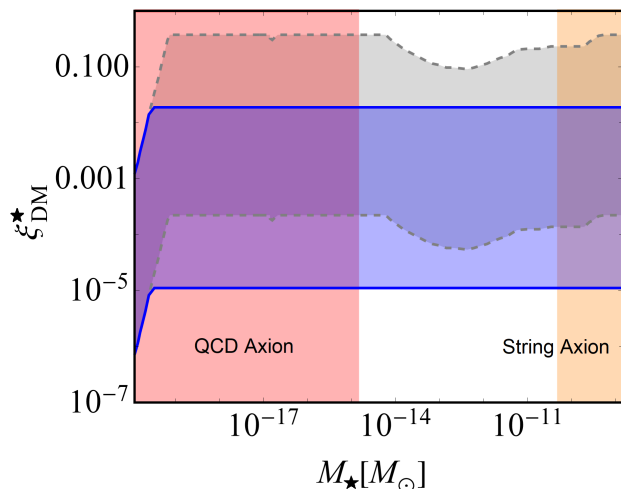


FIG. 3. The blue (gray) shaded band shows the estimate of the current fraction of dark matter in axion stars  $\xi_{\text{DM}}^*$  by using Eq. (17), a fraction in PBHs no greater than 0.5% (10%), a nucleation time of  $z_\star \sim 800$ , and the contour-level  $(m_a v_a R_{\text{halo}}, m_a v_a^2 \tau_{\text{gr}}) \sim (10^2, 10^6)$  at  $z = z_{\text{eq}}$  in the parameter space  $(M_{\text{PBH}}, M_\star)$ . Red (orange) band corresponds to the mass range of axion stars associated with the QCD (string) axion.

ment this picture.

The local dark matter density around a few hundred parsecs around the Sun is  $\rho_{\text{DM}}^{\text{local}} \sim 0.3 \text{ GeV cm}^{-3}$ . Thus, the total local number of axion stars can be expressed as

$$N_{\star, \text{local}}^{\text{total}} \simeq 10^{11} \left( \frac{\xi_{\text{DM}}^*}{0.03} \right) \left( \frac{10^{-11} M_\odot}{M_\star} \right) \left( \frac{r}{100 \text{ pc}} \right)^3. \quad (18)$$

From Fig. 2, take  $M_\star \sim 10^{-18} M_\odot$  ( $M_\star \sim 10^{-10} M_\odot$ ) as the typical mass of axion stars for the QCD (string) axion. Taking a conservative 0.5% in the fraction of dark matter in axion stars, we have up to  $\sim 10^{17}$  ( $10^9$ ) axion stars around our Sun in a radius of 100 pc for the QCD (string) axion.<sup>5</sup>

The number of encounters between the Earth and an axion star per unit of time can be calculated as

$$N_{\otimes \star} = n_{\star, 0}^{\text{local}} \sigma_{\text{eff}} v_{\text{rel}}, \quad (19)$$

where  $n_{\star, 0}^{\text{local}} = \xi_{\text{DM}}^* \rho_{\text{DM}, \text{local}} / M_\star$  is the local number density of axion stars,  $\sigma_{\text{eff}}$  is the usual geometrical cross section for the encounter between the Earth and an axion star enhanced by gravitational focusing, and  $v_{\text{rel}} \simeq 3 \times 10^2 \text{ km/s}$  is the relative velocity between both astrophysical objects. For the axion star radius, we consider the relation  $R_\star \simeq 2 \text{ km} (10^{-10} M_\odot / M_\star) (10^{-5} \text{ eV} / m_a)^2$  [47].

Taking a conservative 0.5% in the fraction of dark matter in axion stars with a typical mass  $M_\star \sim 10^{-18} M_\odot$  ( $M_\star \sim 10^{-10} M_\odot$ ) for the QCD (string) axion case, the number of encounters results to be  $N_{\otimes \star} \sim 10^{-1} \text{ Myr}^{-1}$  ( $N_{\otimes \star} \sim 10^{-3} \text{ Myr}^{-1}$ ). Hence chances of direct detection of dark matter by the Earth passing through an axion star is extremely small.

However, if a non-negligible number of axion stars survive tidal disruptions, then their presence today within the Milky Way halo would enhance DM indirect detection experiments.<sup>6</sup>

## ACKNOWLEDGMENTS

T. T. Y. is supported in part by the China Grant for Talent Scientific Start-Up Project and the JSPS Grant-in-Aid for Scientific Research No. 16H02176, No. 17H02878, and No. 19H05810 and by World Premier International Research Center Initiative (WPI Initiative), MEXT, Japan. M. P. H. is supported in part by National Science Foundation grant PHY-1720332.

\*mark.hertzberg@tufts.edu

†edschiap@uc.cl

‡tsutomu.tyanagida@ipmu.jp

- 
- [1] R. D. Peccei and H. R. Quinn, Phys. Rev. Lett. **38**, 1440 (1977), [328(1977)].
  - [2] S. Weinberg, Phys. Rev. Lett. **40**, 223 (1978).
  - [3] F. Wilczek, Phys. Rev. Lett. **40**, 279 (1978).
  - [4] E. Kiritsis, *Proceedings, 2nd International Conference on New Frontiers in Physics (ICNFP 2013): Kolymbari, Crete, Greece, August 28-September 5, 2013*, EPJ Web Conf. **71**, 00068 (2014), arXiv:1408.3541 [hep-ph].
  - [5] C. J. Hogan and M. J. Rees, Phys. Lett. **B205**, 228 (1988).
  - [6] E. W. Kolb and I. I. Tkachev, Phys. Rev. Lett. **71**, 3051 (1993), arXiv:hep-ph/9303313 [hep-ph].
  - [7] J. Enander, A. Pargner, and T. Schwetz, JCAP **1712**, 038 (2017), arXiv:1708.04466 [astro-ph.CO].
  - [8] M. Kawasaki, K. Saikawa, and T. Sekiguchi, Phys. Rev. **D91**, 065014 (2015), arXiv:1412.0789 [hep-ph].
  - [9] R. Davis, Physics Letters B **180**, 225 (1986).
  - [10] D. H. Lyth, Phys. Lett. **B275**, 279 (1992).
  - [11] M. Axenides, R. H. Brandenberger, and M. S. Turner, Phys. Lett. **126B**, 178 (1983).
  - [12] D. Seckel and M. S. Turner, Phys. Rev. **D32**, 3178 (1985).
  - [13] A. D. Linde, Phys. Lett. **158B**, 375 (1985).

---

<sup>5</sup> This estimate needs to be taken with cautious since we are not taking into account tidal disruptions coming from galactic disk crossing and the Milky Way mean field potential.

---

<sup>6</sup> See [59–61] for astrophysical signatures coming from collisions between axion and neutron stars and [62] for photon emission via parametric resonance.

- [14] A. D. Linde and D. H. Lyth, Phys. Lett. **B246**, 353 (1990).
- [15] M. S. Turner and F. Wilczek, Phys. Rev. Lett. **66**, 5 (1991).
- [16] D. H. Lyth, Phys. Rev. **D45**, 3394 (1992).
- [17] M. Kawasaki, T. T. Yanagida, and K. Yoshino, JCAP **1311**, 030 (2013), arXiv:1305.5338 [hep-ph].
- [18] S. L. Liebling and C. Palenzuela, Living Reviews in Relativity **15**, 6 (2012).
- [19] D. Horvat and A. Marunovi, Class. Quant. Grav. **30**, 145006 (2013), arXiv:1212.3781 [gr-qc].
- [20] G. Choi, H.-J. He, and E. D. Schiappacasse, JCAP **1910**, 043 (2019), arXiv:1906.02094 [astro-ph.CO].
- [21] D. Guerra, C. F. B. Macedo, and P. Pani, JCAP **1909**, 061 (2019), arXiv:1909.05515 [gr-qc].
- [22] A. H. Guth, M. P. Hertzberg, and C. Prescod-Weinstein, Phys. Rev. **D92**, 103513 (2015), arXiv:1412.5930 [astro-ph.CO].
- [23] E. D. Schiappacasse and M. P. Hertzberg, JCAP **1801**, 037 (2018), [Erratum: JCAP1803,no.03,E01(2018)], arXiv:1710.04729 [hep-ph].
- [24] M. P. Hertzberg and E. D. Schiappacasse, JCAP **1808**, 028 (2018), arXiv:1804.07255 [hep-ph].
- [25] L. Visinelli, S. Baum, J. Redondo, K. Freese, and F. Wilczek, Phys. Lett. **B777**, 64 (2018), arXiv:1710.08910 [astro-ph.CO].
- [26] S. Hawking, Mon. Not. Roy. Astron. Soc. **152**, 75 (1971).
- [27] B. J. Carr and S. W. Hawking, Mon. Not. Roy. Astron. Soc. **168**, 399 (1974).
- [28] B. J. Carr, Astrophys. J. **201**, 1 (1975).
- [29] M. Kawasaki, N. Sugiyama, and T. Yanagida, Phys. Rev. **D57**, 6050 (1998), arXiv:hep-ph/9710259 [hep-ph].
- [30] J. Garcia-Bellido, A. D. Linde, and D. Wands, Phys. Rev. **D54**, 6040 (1996), arXiv:astro-ph/9605094 [astro-ph].
- [31] B. P. Abbott *et al.* (LIGO Scientific, Virgo), Phys. Rev. Lett. **116**, 061102 (2016), arXiv:1602.03837 [gr-qc].
- [32] D. G. Levkov, A. G. Panin, and I. I. Tkachev, Phys. Rev. Lett. **121**, 151301 (2018), arXiv:1804.05857 [astro-ph.CO].
- [33] E. Bertschinger, Astrophys. J. Suppl. **58**, 39 (1985).
- [34] K. J. Mack, J. P. Ostriker, and M. Ricotti, Astrophys. J. **665**, 1277 (2007), arXiv:astro-ph/0608642 [astro-ph].
- [35] M. Ricotti, J. P. Ostriker, and K. J. Mack, Astrophys. J. **680**, 829 (2008), arXiv:0709.0524 [astro-ph].
- [36] V. S. Berezhinsky, V. I. Dokuchaev, and Yu. N. Eroshenko, JCAP **1311**, 059 (2013), arXiv:1308.6742 [astro-ph.CO].
- [37] O. Erken, P. Sikivie, H. Tam, and Q. Yang, Phys. Rev. **D85**, 063520 (2012), arXiv:1111.1157 [astro-ph.CO].
- [38] B. Eggemeier and J. C. Niemeyer, Phys. Rev. **D100**, 063528 (2019), arXiv:1906.01348 [astro-ph.CO].
- [39] N. Aghanim *et al.* (Planck), (2018), arXiv:1807.06209 [astro-ph.CO].
- [40] G. G. Raffelt, *Axions: Theory, cosmology, and experimental searches. Proceedings, 1st Joint ILIAS-CERN-CAST axion training, Geneva, Switzerland, November 30-December 2, 2005*, Lect. Notes Phys. **741**, 51 (2008), [51(2006)], arXiv:hep-ph/0611350 [hep-ph].
- [41] M. e. a. P. D. G. Tanabashi, Phys. Rev. D **98**, 030001 (2018).
- [42] M. Kawasaki and T. Yanagida, Prog. Theor. Phys. **97**, 809 (1997), arXiv:hep-ph/9703261 [hep-ph].
- [43] P. Svrcek and E. Witten, JHEP **06**, 051 (2006), arXiv:hep-th/0605206 [hep-th].
- [44] J. Adamek, C. T. Byrnes, M. Gosenca, and S. Hotchkiss, Phys. Rev. **D100**, 023506 (2019), arXiv:1901.08528 [astro-ph.CO].
- [45] E. Seidel and W.-M. Suen, Phys. Rev. Lett. **72**, 2516 (1994), arXiv:gr-qc/9309015 [gr-qc].
- [46] L. Hui, J. P. Ostriker, S. Tremaine, and E. Witten, Phys. Rev. **D95**, 043541 (2017), arXiv:1610.08297 [astro-ph.CO].
- [47] H.-Y. Schive, M.-H. Liao, T.-P. Woo, S.-K. Wong, T. Chiueh, T. Broadhurst, and W. Y. P. Hwang, Phys. Rev. Lett. **113**, 261302 (2014), arXiv:1407.7762 [astro-ph.GA].
- [48] D. G. Levkov, A. G. Panin, and I. I. Tkachev, Phys. Rev. Lett. **118**, 011301 (2017), arXiv:1609.03611 [astro-ph.CO].
- [49] B. J. Carr, K. Kohri, Y. Sendouda, and J. Yokoyama, Phys. Rev. **D81**, 104019 (2010), arXiv:0912.5297 [astro-ph.CO].
- [50] A. Barnacka, J.-F. Glicenstein, and R. Moderski, Physical Review D **86** (2012), 10.1103/physrevd.86.043001.
- [51] P. W. Graham, S. Rajendran, and J. Varela, Phys. Rev. **D92**, 063007 (2015), arXiv:1505.04444 [hep-ph].
- [52] H. Niikura *et al.*, Nat. Astron. **3**, 524 (2019), arXiv:1701.02151 [astro-ph.CO].
- [53] P. Tisserand *et al.* (EROS-2), Astron. Astrophys. **469**, 387 (2007), arXiv:astro-ph/0607207 [astro-ph].
- [54] K. Inomata, M. Kawasaki, K. Mukaida, Y. Tada, and T. T. Yanagida, Phys. Rev. **D96**, 043504 (2017), arXiv:1701.02544 [astro-ph.CO].
- [55] E. W. Kolb and I. I. Tkachev, Astrophys. J. **460**, L25 (1996), arXiv:astro-ph/9510043 [astro-ph].
- [56] M. Fairbairn, D. J. E. Marsh, J. Quevillon, and S. Rozier, Phys. Rev. **D97**, 083502 (2018), arXiv:1707.03310 [astro-ph.CO].
- [57] M. P. Hertzberg, E. D. Schiappacasse, and T. T. Yanagida, (2019), arXiv:1910.10575 [astro-ph.CO].
- [58] C. P. d. los Heros (2020) arXiv:2001.06193 [astro-ph.HE].
- [59] A. Iwazaki, Phys. Rev. **D91**, 023008 (2015), arXiv:1410.4323 [hep-ph].
- [60] S. Raby, Phys. Rev. **D94**, 103004 (2016), arXiv:1609.01694 [hep-ph].
- [61] T. Dietrich, F. Day, K. Clough, M. Coughlin, and J. Niemeyer, Mon. Not. Roy. Astron. Soc. **483**, 908 (2019), arXiv:1808.04746 [astro-ph.HE].
- [62] M. P. Hertzberg and E. D. Schiappacasse, JCAP **1811**, 004 (2018), arXiv:1805.00430 [hep-ph].